Journal Pre-proofs

Molecular engineering of thixotropic, sprayable fluids with yield stress using associating polysaccharides

Yu-Jiun Lin, Jeffrey Horner, Brandon Illie, Matthew L. Lynch, Eric M. Furst, Norman J. Wagner

PII: S0021-9797(20)30852-3
DOI: https://doi.org/10.1016/j.jcis.2020.06.107
Reference: YJCIS 26604

To appear in: *Journal of Colloid and Interface Science*

Received Date: 22 April 2020
Revised Date: 16 June 2020
Accepted Date: 24 June 2020

Please cite this article as: Y-J. Lin, J. Horner, B. Illie, M.L. Lynch, E.M. Furst, N.J. Wagner, Molecular engineering of thixotropic, sprayable fluids with yield stress using associating polysaccharides, *Journal of Colloid and Interface Science* (2020), doi: https://doi.org/10.1016/j.jcis.2020.06.107

This is a PDF file of an article that has undergone enhancements after acceptance, such as the addition of a cover page and metadata, and formatting for readability, but it is not yet the definitive version of record. This version will undergo additional copyediting, typesetting and review before it is published in its final form, but we are providing this version to give early visibility of the article. Please note that, during the production process, errors may be discovered which could affect the content, and all legal disclaimers that apply to the journal pertain.

© 2020 Published by Elsevier Inc.

Graphical Abstract

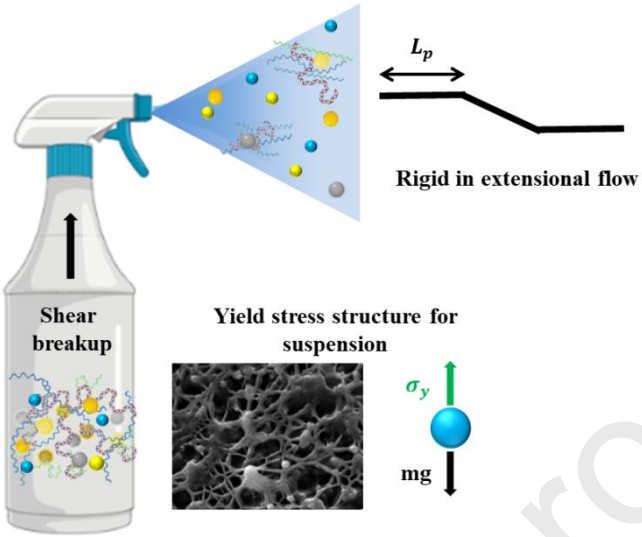

Journal Pre-proofs

Journal Pre-proofs

Molecular engineering of thixotropic, sprayable fluids with yield stress using associating polysaccharides

Yu-Jiun Lin[1], Jeffrey Horner[1], Brandon Illie[2], Matthew L. Lynch[2], Eric M. Furst[1], and Norman J. Wagner[1]

[1]Center for Research in Soft Matter and Polymers, Department of Chemical and Biomolecular Engineering, University of Delaware, Newark, DE 19716

[2]The Procter & Gamble Company, Cincinnati, OH 45224

Abstract

Hypothesis

Molecular engineering facilitates the development of a complex fluid with contradictory requirements of yield stress and sprayability, while minimizing the amount of structuring material (< 0.05 wt%). This unique system can be achieved by a biopolymer hydrogel with tunable inter- and intra-molecular interactions for microstructural robustness and molecular extensibility by the variation of chemical conformations that microstructure breaks up under shear followed by a low molecularly extensible response.

Experiments

Blends of xanthan and konjac glucomannan containing 99.95 wt% water are demonstrated to satisfy these contradictory requirements and formulated as a function of KCl concentrations. A systematic study was performed using shear and extensional rheology and compared to a reference solution of polyethylene oxide (PEO), a well-known, Boger fluid, highlights the role of molecular elasticity in controlling critical rheological properties. Static light scattering (SLS) and simultaneous rheology and

Journal Pre-proofs

small-angle neutron scattering (RheoSANS) are also used to elucidate the equilibrium structure and flow dynamics.

Findings

The blends exhibit a lower yield stress and extensional resistance with added KCl, which leads to good spray characteristics in contrast to strain-hardening PEO. The results suggest that the inter-molecular attractions between the two gums leading to network formation with appropriate stiffness that break up readily under shear and low molecular elasticity are critical molecular design parameters necessary to achieve sprayable, yields stress fluids.

Keywords: hydrogel, molecular extensibility, yield stress fluid, sprayable, xanthan, konjac glucomannan, polyethylene oxide, microfluidics, rheology, suspension stability

1. Introduction

Successful industrial and consumer applications of structured fluids often simultaneously require seemingly contradictory attributes. A common example with consumer products is the need for long-term shelf and transportation stability coupled with the requirement for customer-acceptable dispensing [1]. Stability often entails suspending dispersed particles and emulsions against creaming and sedimentation for months under a range of temperatures and stress conditions, and recovery of this property after agitation; dispensing can vary from pouring from a bottle to spraying from a nozzle [1, 2]. Moreover, the same contradictions extend to a vast scope of implementations including paints [3], injectable medicine [4], sprayable hydrogel drug [5-8], and fabric refreshers [1]. Satisfying all of

Journal Pre-proofs

these product attributes necessitates a molecular level understanding of, and control over, the formulation of industrially useful structured fluids.

A key property of structured fluids necessary across a broad range of applications is the yield stress [9]. Broadly, structured fluids can be prepared from particulate or polymeric, reversibly-associating "building blocks" including clay gels, fat particles, emulsions, microgels, and polymeric gels [2, 9, 10]. At rest, associations between components create space-spanning microstructures that can support stress, while under flow, the associations break (reversible) and the flow properties are governed by the remaining building blocks or domains. Importantly, upon flow cessation the structure responsible for the yield stress must rebuild faster than significant creaming or sedimentation.

Of concern here are yield stress fluids suitable for suspending components in typical consumer products, such as functional particles in a pourable or sprayable aqueous formulation. A simple force balance suggests that to suspend a particle with a diameter d, the yield stress has to satisfy the criterion that $\sigma_y \geq C\Delta\rho g d$, where $\Delta\rho$ is the difference in the density between the particle and the fluid, g is the gravitational constant, and the semi-empirical constant $C = 3$ [11]. For example, to stabilize a ~50-μm particle with a density difference of ~0.1 g/cm^3, the yield stress needs to be above ~0.15 Pa. While this is a modest value of yield stress in comparison to other applications such as the whipped cream containing ~30 Pa to maintain the shape [2], a technical challenge for many consumer products is that the structuring agents that generate this yield stress are required to be present in low concentrations, often less than a weight percent. A recent review highlights the methodology

Journal Pre-proofs

necessary to design such systems using molecular attractions and polyelectrolytes, as well as the lack of predictive models, which therefore necessitates further experimental studies of model systems to guide formulation and improve our molecular-level understanding [9].

The second key feature of structured fluids is the desired flow property of the yield stress fluid during dispensing. Dispensing involves more complex flows, which are often strong extensional flows, such as observed during spraying [12]. Polymer solutions with significant molecular elasticity can exhibit extensional thickening, which can prevent effective pouring and spraying [13, 14]. Flexible polymers are extensible and stretch when the imposed hydrodynamic drag exceeds the entropic elasticity of the molecule under an elongational flow [15]. This molecular extensibility causes unwanted extensional resistance of the polymer solution [13, 16].

To illustrate these phenomena and motivate the following study, representative images of dilute solutions of polymer gels containing 0.02 wt% xanthan and 0.03 wt% konjac glucomannan, (Xg/Kg) in water containing ~30 micron sized particles of polyethylene with density about 0.5% greater than water are shown. The Xg/Kg solution has sufficient yield stress to stabilize while particles, which otherwise rapidly sediment in water, as shown in Figure 1a. However, spraying this same Xg/Kg solution using a commercial spray bottle yields a fine mist, which is the desired outcome Figure 1c, whereas adding a weight percent of relatively low Mw, flexible polymer, PEO, leads to highly undesirable string formation, Figure 1b.

Journal Pre-proofs

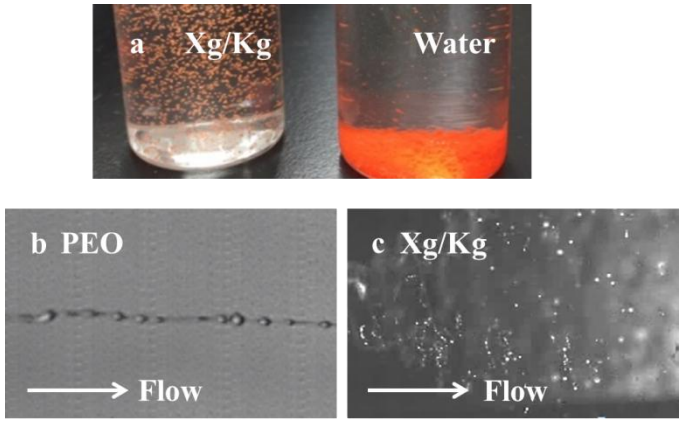

Figure 1 (a) Left: 32-38 μm polyethylene particles in associating polysaccharides (0.02 wt% xanthan + 0.03 wt% konjac glucomannan, Xg/Kg); Right: settled particles in water. (b) The liquid stream of the sprayed 1wt% 1000K Mw PEO solution. (c) Sprayed droplets of Xg/Kg. Flow direction is from left to right.

In the following, an improved understanding of how to tune the molecular properties of structured gum solutions to build a suitable yield stress at low shear rates while having high shear flowability and low extensional elasticity is achieved through a combination of rheological and microstructural characterization. This understanding is furthered by contrasting these results with similar measurements on a model Boger fluid consisting of a polyethylene oxide (PEO) solution. This comparison leads to the hypothesis that the relatively stiff polymer gum complex assembles into a space spanning structure sufficiently strong to form a yield stress, but which can reversibly dissociate under a high shear or extension deformation rate, resulting in flowability and low extensional elasticity suitable for spray dispensing.

2. Material and Methodology

2.1 Materials

Journal Pre-proofs

Xanthan-konjac glucomannan (0.02 wt% - 0.03 wt%) gum solutions (Xg/Kg) were supplied by Procter & Gamble (P&G). Xanthan gum is purchased from KELTROL® CC (Atlanta, GA) and konjac gum is supplied by FMC Corporation (Nutricol® XP 3464 Konjac Flour, Philadelphia, PA). The Xg/Kg is pretreated under 1811g centrifuge for 10 mins to remove undissolved polysaccharides. The percentage of dried sediments in the remaining unused fluid is also measured by HR73 Halogen Moisture Analyzer (METTLER, TOLEDO) and the result is 0.05 ±0.007 wt%. Molar mass and the ratio of acetylated to non-acetylated is 4500 – 6000 kDa and 0.25 – 1.0 for xanthan (Xg), respectively, and 1000 – 2000 kDa and 0 – 0.5 for konjac (Kg), respectively. Potassium chloride is added into the pretreated Xg/Kg to form 0.1 M and 0.5 M KCl solutions, and the solutions are stirred at room temperature by a roll mixer at least overnight. H_2O is replaced by D_2O in the samples for the neutron scattering study.

Polyethylene oxide (PEO, 2000 kDa) is dissolved in a 1:2 weight ratio water:glycerol mixture and stirred by a magnetic bar at 50 ^{o}C overnight. The concentration (c) is made to be $3.5c^* < c_e$, and therefore $c = 0.3$ wt%, where $c^*$is the the overlap concentration and c_e~$10c^*$ is the entanglement concentration [17]. The intrinsic viscosity $[\eta]$ is calculated based on the Mark-Houwink-Sakurada equation $[\eta] = 0.072M_W^{0.65}$, where M_W is the molecular weight. The overlap concentration is estimated by the equation $c^* = 0.77/[\eta]$ [18]. Deionized water (resistivity 18.2MΩ•cm) was used. The free-draining Rouse model, with its consideration of localized drag forces along the polymer chain, is applied to estimate the characteristic Rouse relaxation time for solutions ($c > c^*$) using the

equation $\tau_{\lambda R\_PEO} = \frac{6[\eta]M_W\eta_s}{\pi^2 RT}$ [19]. The Rouse relaxation time for this PEO solution is calculated to be 8.4 ms.

2.2 Shear rheology

A strain-controlled ARES-G2 rheometer equipped with parallel-plate geometry (TA Instruments) is used. Parallel-plate geometry is often recommended for probing cross-linked hydrogels with micron-size filaments to adjust the height between plates and avoid confinement effects [20]. The minimum torque (T_{min}) in steady shear is 0.1 μN·m and 0.05 μN·m in oscillation. This minimum torque is used to identify a minimum measurable viscosity using the equation $\eta > F_\tau T_{min}/\dot{\gamma}$ and the minimum stress is estimated to be 4.07×10^{-3} Pa, and F_τ = 40744 Pa·(N·m)$^{-1}$ is the stress constant for the rheological tool of interest. Instrument inertia is calculated using the equation $G > \varepsilon\omega^2(IF_\tau/F_r)$, where $F_r = 62.5$ rad^{-1}, $IF_\tau/F_r = 5.46\times10^{-3}$ Pa·s^2, and $\varepsilon = 0.01$ [21]. All experiments were performed at 25 ^{o}C. Shear rates were probed stepwise with the steady flow curves reported during the descending branch of a protocol comprised of ascending steps followed by descending steps. Small amplitude oscillatory shear (SAOS) measurements were performed in the linear regime at 10% strain. The minimum measurable dynamic modulus is calculated from the minimum torque using the equation $G_{min} = F_\tau T_{min}/\gamma_0$.

2.3 Microfluidics and particle image velocimetry (PIV)

Journal Pre-proofs

A microfluidic platform offers additional capabilities to obtain extensional flow properties [22-24]. Extensional rheology is measured using a hyperbolic contraction-expansion, depicted in Figure 2, with dimensions: h = 100 μm, l_c = 3000 μm, L_1 = 6000 μm, L_2 = 12000 μm, w_c = 99.5 μm, and w_u = 2000 μm. For this device, the Hencky strain is $\varepsilon_H = 3$ as calculated from $\varepsilon_H(x) = \ln\left(\frac{w_u}{w(x)}\right)$. The device was fabricated using a SU-8 2035 (Microchem Corp) photoresist template as a 100-micron tall designed pattern. A liquid polydimethylsiloxane (PDMS) (Sylgard 184, Dow Corning), mixed in a 10:1 ratio of elastomer base to curing agent, was poured onto the SU-8 mold, cured at 150°C for 10 minutes, and removed to form a patterned PDMS layer. The PDMS layer and a clean glass slide were bonded by treating with O_2 plasma. A similar PDMS microchannel has been reported to have less than 7% deformation under pressure below 100 kPa after a temperature treatment of 200°C [25]. The measured pressure is under 65 kPa in the measurements reported in the paper.

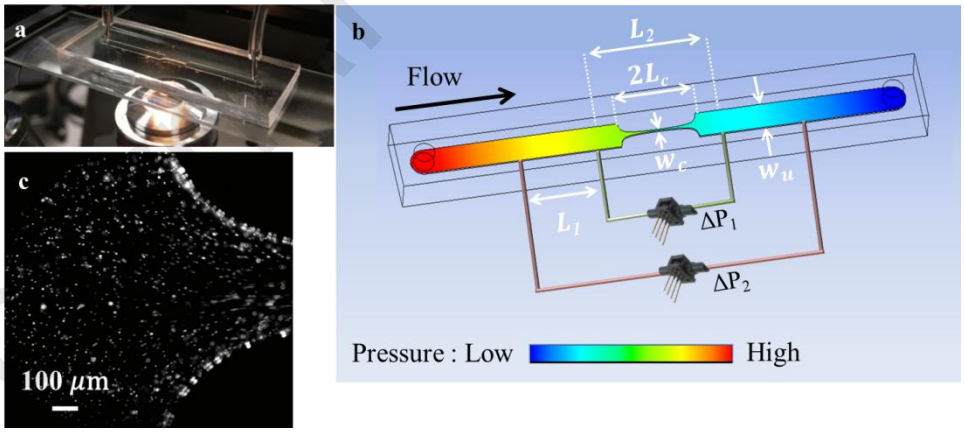

Figure 2 (a) Illustration of a PDMS microchannel. (b) The design of a microfluidic hyperbolic channel and a qualitative pressure drop is shown via color map. (c) An image of fluorescent particles in the channel entry used for PIV.

Fluids are injected by a syringe pump (Harvard Apparatus PHD 2000) using 1 mL and 10 mL gastight Luer Lock glass syringes (SGE Analytical Science). The flowrate (Q) ranges from 1.885 to 1885 μL·min^{-1} and ±1% error is expected from the dispensing of the syringe. A metal ceramic heater (20 mm × 20 mm, Thorlabs) is attached on the bottom of the device near the inlet to maintain the temperature around 25 ^{o}C over the contraction-expansion unit. The gradient of the temperature over the entire device is ±1 ^{o}C. PDMS is reported to have nanometer scale of adsorption layer of polysaccharide and PEO. Compared to the micro-scale dimensions used in the design, the effect on fluid behavior is neglected [26, 27]. The microfluidic device was staged on an inverted microscope (Eclipse TE2000-U, Nikon), and the images recorded using a high-speed camera, (Phantom V5.1, Vision Research, Inc.) using epifluorescence microscopy, and processed by an open-source particle image velocimetry code (PIVlab) to generate velocity profiles [28]. The gradients of the velocity profile are computed using ParaView 5.6.0 by the method of gradient of unstructured dataset [29]. Two differential pressure transducers (operating range: 5 and 15 psi, 26PC series, Honeywell) are used to measure the corresponding pressure drop across the micro-geometries as shown qualitatively in Figure 2b. Transducers are calibrated using a microfluidic flow control system (MFCS^{TM}-EZ, Fluigent), and a linear relationship between measured voltage and pressure drop is found as plotted in Figure S1. Fluoresbrite® Microspheres 3.00µm (4.55 x 10^{10} particles/ml) were seeded and diluted to be 0.025wt% in solutions as tracers to visualize the flow streamline over the mid-plane of the channel as demonstrated in Figure 2c. Tracer particles are also used to examine the possibility of the upstream

Journal Pre-proofs

vortex caused by the elastic instability, and no vortex is found within the testing window of the flow rates in this geometry. The addition of 0.025 wt% of fluorescent microspheres does not change the material rheology. The Hencky strain and the nominal extensional rate ($\dot{\varepsilon}_H$) in the centerline of the contraction and expansion is determined from the equation $\dot{\varepsilon}_H = \frac{Q}{l_c h}\left(\frac{1}{w_c} - \frac{1}{w_u}\right)$. The calculation for the extensional contribution to the measured pressure drop and the resultant extensional viscosity are shown in Supplementary Material S2 [23]. Also, an example of imaging analysis for Xg/Kg without added KCl flowing at $\dot{\varepsilon}_H = 1$ 1/s in the microfluidic channel is presented in Supplementary Material S2. To examine the relative significance of inertia, the Reynolds number $Re = \rho d_h V_c/\eta(\dot{\gamma})$ is calculated, where ρ is the fluid density, $d_h = 2hw_c/(h + w_c) = 99.75$ μm is the hydraulic diameter, $V_c = l_c\dot{\varepsilon}_H$ is the characteristic velocity. The range of the Reynolds number is listed in Table 1.

Table 1 Reynolds number for Xg/Kg and 2000K PEO in the microfluidic device

Solution	Re
Xg/Kg 0 M KCl	1.7×10^{-3}-3.4×10^{1}
Xg/Kg 0.1 M KCl	3.2×10^{-3}-4.7×10^{1}
Xg/Kg 0.5 M KCl	4.6×10^{-3}-9.7×10^{1}
2000K PEO	3.7×10^{-3}-3.7×10^{0}

2.4 Transient Extensional Rheology

Transient extensional rheology is measured using a filament pulling rheometer (VADER-1000, Rheo Filament ApS). The calculation of the extensional stress ($\langle\sigma_{zz} - \sigma_{rr}\rangle$) over the mid-plane of the testing fluid and the extensional stress growth coefficient ($\overline{\eta_E^+}$) is provided in Supplementary Material S3.

2.5 Static Light Scattering and RheoSANS

Journal Pre-proofs

Static light scattering (SLS) is performed using 3D LS Spectrometer (LS Instruments AG, Switzerland) with a wavelength of 660 nm at 25 ^{o}C at scattering angles of 15 to 135^{o}. Simultaneous small-angle neutron scattering and rheological (RheoSANS) measurements were performed on the NG3 vSANS diffractometer with Anton-Paar MCR 501 stress-controlled rheometer equipped with a 50 mm cup and 48 mm bob (a quartz Couette geometry) with $\lambda = 6$ Å at the NIST Center (Neutron Research in Gaithersburg, MD, USA). Sphere model and Guinier function are used to find the correlation length of the hydrogel, and the details and fitting parameters of the models are shown in Supplementary Material S4.

3. Results and Discussions

3.1 Material Properties

Knowledge of molecular properties is essential for understanding the contribution of the polymers to the elastic and flow behavior of complex fluids at macro-scale, especially under high deformation rates. The theoretical contour length or fully extended length (L_c), finite extensibility parameter (L_E), and entropic spring force (f_{spring}) are calculated as listed in Table 2. f_{spring} is calculated using the Marko-Siggia law, $f_{spring} = \frac{k_B T}{L_p}\left[\frac{1}{4}\left(1-\frac{R}{L_c}\right)^{-2} - \frac{1}{4} + \frac{R}{L_c}\right]$, where $k_B = 1.38\times10^{-23}$ $(\mathrm{m}^2 \cdot \mathrm{kg})/(\mathrm{s}^2 \cdot \mathrm{K})$ is the Boltzmann constant, T is temperature, R is the spring end-to-end vector, and $\frac{R}{L_c}$ is the fractional extension of the molecule [30, 31].

Journal Pre-proofs

Table 2 Molecular properties of PEO, Xg, and Kg

Chemical		L_p (nm)	Debye screening length (nm)[(a)]	Monomer molar mass (Da)	Theoretical L_c [32] (μm)	Finite extensibility L_E [32]	f_{spring} at $R/L_c =$ 0.7 (pN)
PEO (2000K)		0.37 [33]	-	44.05	5.7	88	36.11[(b)]
Kg		13 [34]	-	666.6	2.5 – 4.9	9.7 – 13.7	1.02
Xg	0M KCl	417 [35]	20.8	933.8	3.9 – 5.3	2.2 – 2.5	0.03
	0.1M KCl	141 [35]	0.96			3.7 – 4.3	0.09
	0.5M KCl	168 [35]	0.43			3.4 – 3.9	0.08

*$L_c = 0.82nl$, $L_E = L_c/\langle R^2\rangle_0^{0.5}$,and $\langle R^2\rangle_0 = 2L_cL_p$ is the mean-squared end-to-end length of a molecule, l is monomer length or bond length (1.54 Å in carbon-carbon bond for PEO, 1 nm for Xg, and 2 nm for Kg), and n is the number of backbone monomers [32].
[(a)]For water, Bjerrum length is 0.71 nm at 300K.
[(b)]This value is consistent with the force range obtained from molecular dynamics simulation [36].

Table 3 Conformational properties of Xg [37]

Xanthan conformation	Average distance between the charged units (nm)	Counterion condensation fraction
Random coil	0.65	0.09
Single helix	0.56	0.21
Double helix	0.28	0.61

Dinic and Sharma characterized two transitions in applications dominated by the extensional flow: inertiocapillary (IC)/viscocapillary (VC) to elastocapillary (EC) and EC to the finite extensibility (FE) effect [14]. Here, for spraying, we hypothesize the second transition for EC to FE dominates; hence our focus is the molecular extensibility of the polymers in solutions. In Table 2, molecular extensibility and the restoring spring force of PEO are found to be an order of magnitude higher than that for either Xg or Kg. These intrinsic quantities have significant effects on the creation of molecular and structural elasticity that eventually gives rise to the resistance in the extensional flow.

Note that the biopolymers, Xg and Kg by themselves are present as rigid or semi-flexible rods in water, respectively, and Kg has higher extensibility than Xg.

To investigate the contribution of molecular elasticity to macro-scale extensional properties, ions are added to control the configuration of Xg. Xg is negatively charged due to pyruvate groups on the trisaccharide sidechain (Figure 3a) and the addition of KCl results in charge screening, thereby reducing the electrostatic repulsion between these charged groups. The Debye screening length is also listed in Table 2 and the average distance between charged units as well as the counterion condensation fraction for different molecular Xg conformations is listed in Table 3. When calculating the screening length, the positive ions (Na^+ and K^+) associated with Xg during the manufacturing process are also considered. The ionic strength of these associated ions is estimated to be 2.1×10^{-4} M with the assumption of a complete dissociation of ions from Xg. Hence, the screening length is 20.8 nm instead of 960 nm in DI water (the case without considering ions from the manufacturing process) [38]. If the Debye screening length is smaller than the distance between the charged units, the charge is screened. Only the screening length of Xg in 0.5M KCl has possible smaller value than the distance between charged units, and therefore a complete screening. De-pyruvated xanthan is also found to form more ordered structure even without electrolytes [39]. Camesano and Wilkinson found that salt screening causes Xg to reorganize into more ordered structures and increases the molecular flexibility by decreasing the persistence length (Figure 3b) [35]. Several molecular conformations of Xg have been proposed including random coils, single helices, and antiparallel double helices, which depend

Journal Pre-proofs

on the physicochemical conditions of the environment [40]. On the other hand, there is no occurrence of strong self-gelation or structure reorientation of uncharged Kg molecules in the presence and the absence of ions [41].

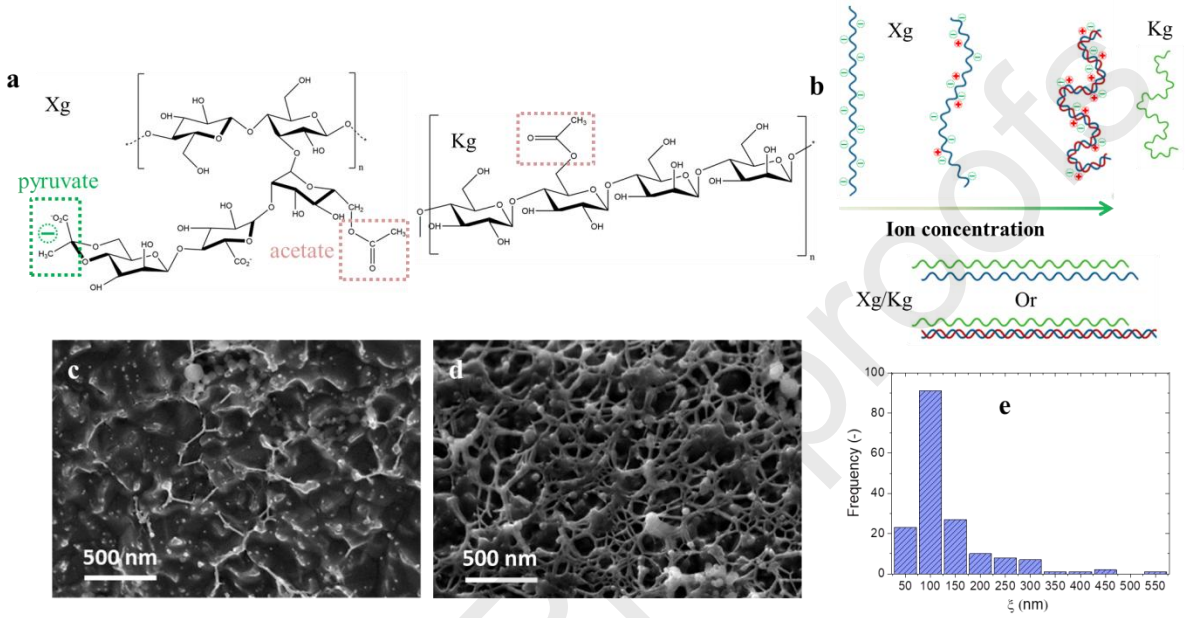

Figure 3 (a) Molecular structures of Xg and Kg. Green box shows the pyruvate group and red boxes represents the acetate group. (b) Illustrations of the secondary structure of Xg with an increased ion concentration and the association of Xg and Kg. Cryo-SEM images of (c) 0.05 wt% Xg (no added salt). (d) 0.05 wt% Xg/Kg (no added salt). (e) Mesh size distribution of 0.05 wt% Xg/Kg (no added salt) processed by ImageJ with the bandpass filter to eliminate the depth effect.

The gelled microstructures of Xg, and self-associated solutions of Xg and Kg are imaged using cryo-SEM. Xg is known to self-associate by hydrogen bonds in water [42]. Xg displays a heterogeneous network and a thinner bundle of molecules in Figure 3c. In contrast, the molecular bundle between Xg and Kg is thicker (Figure 3d) and the mesh size distribution is presented in Figure 3e. Abbaszadeh et al. proposed that Kg interacts and forms a bundle with both formations of single and double helices of Xg by physical interactions [43]. Therefore, the network is not formed by the end-to-end effect

from individual polymers. These physical interactions enable Xg and Kg to form a cross-linked structure and produce a yield stress fluid that is also able to self-heal. Hence, Xg/Kg is a physical hydrogel. Non-linear mechanical responses in both shear and extensional flow are examined in the following sections.

3.2 Equilibrium Structure and Viscoelasticity

Results for the aqueous solutions of Xg/Kg show that the sample is primarily elastic over the frequency range plotted in Figure 4a, characteristic of a gel. Note that the samples do not exhibit terminal behavior, which is consistent with a weak yield-like behavior, but no low frequency plateau in the elastic modulus is evident. The shear modulus can be correlated to a characteristic mesh size (ξ) of a fully swollen gel that the osmotic pressure for expanding is equal to the elastic modulus for preventing expansion by using the relationship $G \cong k_B T/\xi^3$ [44, 45]. Using the elastic modulus at 10^{-2} rad/s, the mesh size is estimated to be $\xi \cong 250$ nm for 0 M KCl. This value is comparable to the mesh size in Figure 3d-e. For both added KCl concentrations, this apparent mesh size increases to $\xi \cong 280$ nm. In addition, the results of SLS and SANS of Xg/Kg in 0M and 0.5M KCl solutions are shown in Figure 5a-b. A characteristic length scale for both solutions is observed in the range of 0.0014 $Å^{-1} < q <$ 0.002 $Å^{-1}$ and the corresponding real space range is 300 nm - 460 nm. Pochan et al. has shown that this characteristic length could be associated with the average long spacing between neighboring self-assembled structures using a combination of cryo-TEM and SANS [46]. Here, we

Journal Pre-proofs

used the sphere model with a polydisperse Schulz distribution function, as well as a Guinier plot for linearized fit ($lnI(q)\ vs\ q^2$), and Kratky plot ($q^2I(q)\ vs\ q$) to find the correlation length in the system. The Guinier plot is presented in Figure 5c over the same q range as in Figure 5a-b, where the plot is according to the linearized equation. The range of the plot corresponding to $qR_g < \sqrt{3}$ shows the probed range ($2\pi/q$) is larger than the particle or domain size, indicating validity of fitting. The peak of Kratky plot is also reported as plotted in Figure 5d. The values of the correlation length are listed in Table 4. The correlation length obtained from various methods lies in a similar range and only cryo-SEM results show a mesh size smaller than 100 nm. The polydispersity (PD) of the structure with 0.5M KCl (PD = 0.90) is much higher than for 0M KCl (PD = 0.44), which suggests that the distribution of the mesh size is broadened by adding KCl. With this estimation of the mesh size, we now know that the screening length (Table 2) is significantly smaller than the characteristic mesh size. Therefore, electrolyte screening can change the local chain flexibility and association, but does not directly affect the network structure on the lengthscale of the observed mesh size.

Table 4 Correlation length of Xg/Kg

Method[a]	0M KCl	0.5M KCl
SANS data	300 - 460	
Cryo-SEM	50 - 550	-
Elastic modulus	250	280
Sphere model	313	215
Guinier model	227	162
Guinier plot	196	164
Kratky plot	374	330

[a]Unit is in nano-meter (nm)

In addition, as a result of the lowering of the persistence length of Xg with the addition of KCl, the moduli drop and the slope of storage and loss moduli in Figure 4a increase, suggesting increased

molecular flexibility [47]. Xg/Kg in 0.1M KCl and 0.5 M KCl shows similar SAOS rheology. Meanwhile, the PEO solutions exhibit terminal behavior over this frequency regime as expected for this semi-dilute concentration, as shown in Figure 4b.

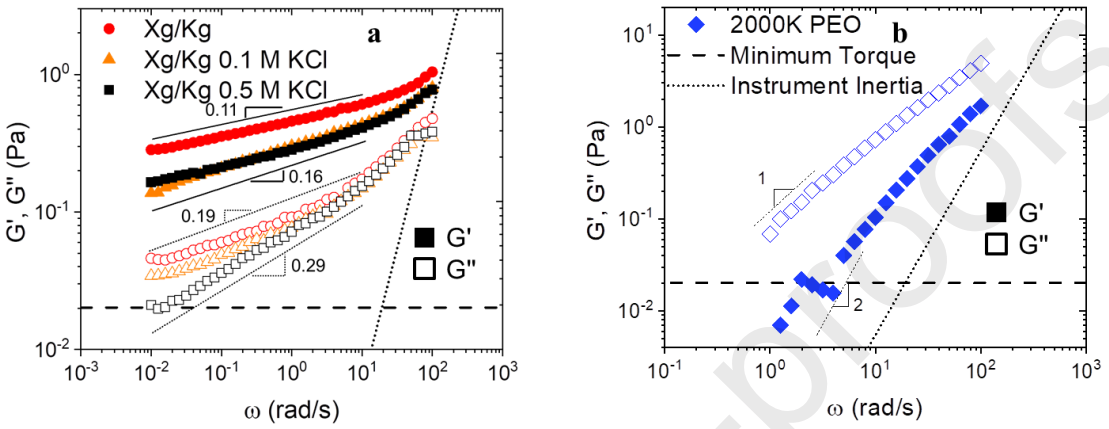

Figure 4 SAOS of aqueous solutions of (a) Xg/Kg with added KCl and (b) 2000K PEO. Power law scalings are shown for reference. The strain amplitude is 10%.

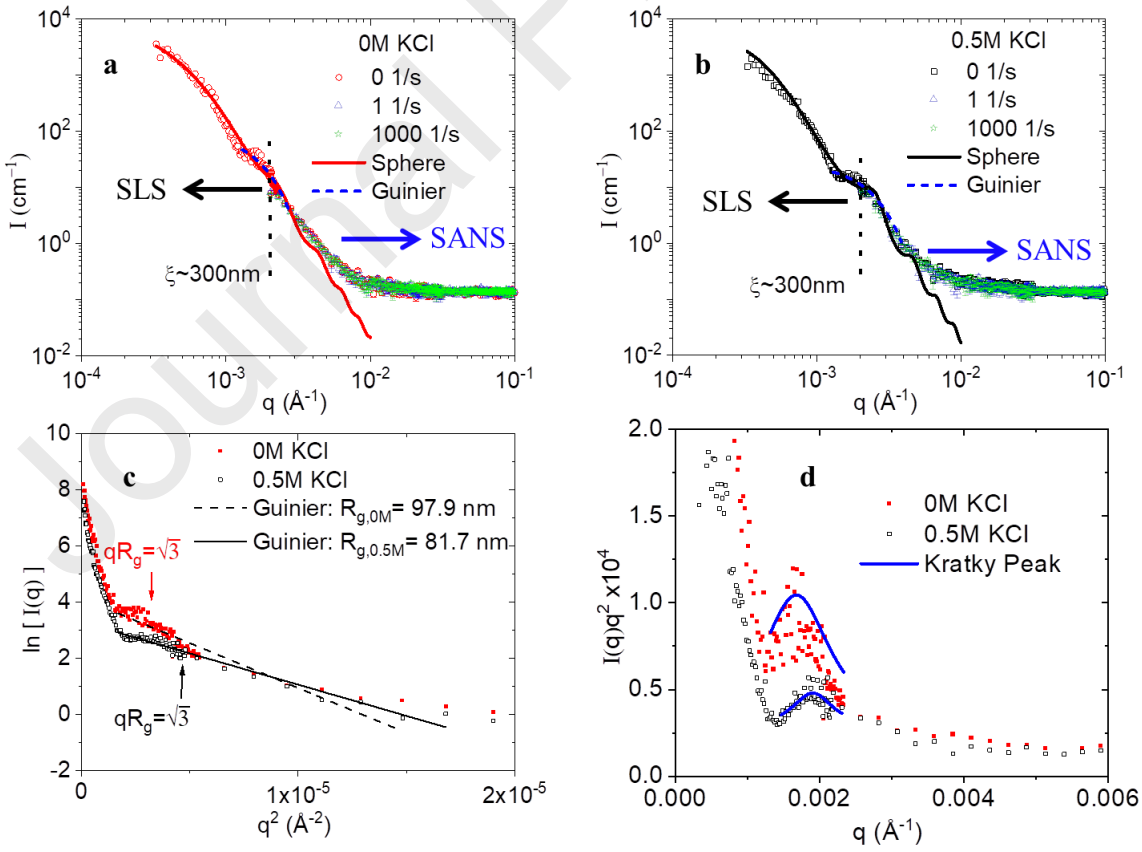

Journal Pre-proofs

Figure 5 SLS and SANS data for (a) Xg/Kg without added KCl and (b) Xg/Kg with added 0.5M KCl. Solid lines are the fitting from a sphere model with the assumption of existed polydispersity and dashed lines are fitting from Guinier model. SANS results also include data under shear rates of 1 and 1000 1/s. (c) Guinier plot and (d) Kratky plot of Xg/Kg with and without added KCl.

3.3 Rheology and Morphology under a Steady Shear Flow

The shear viscosity of Xg in aqueous solution exhibits a Newtonian plateau (~150 mPa·s) under low shear rates ($\dot{\gamma}$<0.1 s^{-1}), followed by a power-law shear thinning, while Kg shows Newtonian behavior (~2 mPa·s), as illustrated in Figure 6a. In contrast, the shear viscosity of Xg/Kg solutions show evidence of a yield-like behavior at low shear rates followed by a strong shear-thinning as presented in Figure 6a. The corresponding shear stress is plotted in Figure 6b with fits to the Herschel-Bulkley model ($\sigma = \sigma_y^{HB} + K\dot{\gamma}^n, \sigma \geq \sigma_y$). The fit values for the dynamic yield stress σ_y^{HB}, consistency parameter, and power law parameters are listed in Table 5. The yield stress is observed to decrease with increased concentrations of KCl.

Table 5 Fitting parameters of Herschel-Bulkley model

Parameter	0M KCl	0.1M KCl	0.5M KCl
σ_y^{HB} (Pa)	0.153±0.009	0.150±0.003	0.118±0.004
n	0.623±0.008	0.789±0.005	0.846±0.009
K(Pa-s^n)	0.098±0.005	0.019±0.001	0.007±0.001

The molecular associations of Xg presented previously also influence the molecular association between Xg and Kg. The strength of the Xg/Kg gel depends on the number of the active sites on the Xg and these sites can be occupied by adsorbed ions, inducing a weaker gel. Annable et al. note that cations can promote Xg self-association at the expense of Xg-Kg interactions by charge-screening

effect because Xg is negatively charged and Kg is uncharged [41]. By adding 0.5M KCl, there is significant Manning counterion condensation (0.61) as listed in Table 3 [37], which would weaken the xanthan-konjac association by reducing the net charge on the xanthan.

With increasing KCl, the viscosity at the highest shear rate, 1000 s^{-1}, decreases from 7.73 to 3.03 mPa·s. RheoSANS results presented in Figure 5a-b, demonstrate that the structure below 300 nm remain unchanged for shear rates from 0 to 1000 s^{-1}. Also, both the minimal values in Herman's orientation function (Eq. 1 and Table 6) and 2D scattering patterns lacking anisotropy (Figure 6c) show that the network was not stretched and oriented. Therefore, these observations indicate that the network structure breaks up by rupturing a larger length-scale structure structure beyond 300 nm, the limit probed by rheoSANS, without strong orientation. Similar behavior is also reported for peptide hydrogels [4] and carbon black suspensions [48]. The shear viscosity obtained from rheoSANS measurements also confirm that using a D_2O solution has negligible effects on the rheological properties. Further, the Cox-Merz rule plotted in Figure 6d failed, as expected, showing that the structure of network indeed changes under shear flow because the steady shear viscosity is lower than the complex viscosity measured at equilibrium. In contrast, the shear viscosity of 2000K PEO solution is nearly shear-independent over this range of shear rates. Simulations indicate that the flexible PEO molecules are tumbling and stretched by hydrodynamic drag forces under shear flow [49].

Journal Pre-proofs

$$f = \frac{3\langle\cos^2\phi\rangle - 1}{2}, \text{ in which } \langle\cos^2\phi\rangle = \frac{\int_0^{\frac{\pi}{2}} I(\phi)\cos^2\phi\sin\phi d\phi}{\int_0^{\frac{\pi}{2}} I(\phi)\sin\phi d\phi} \qquad (1)$$

where f is the Herman's orientation function, I(ϕ) is annular averaged scattering intensity, and ϕ is the azimuthal angle [4].

Table 6 Herman's orientation function

Conc. of KCl		0M	0.5M
$\dot{\gamma}$ $(1/s)$	0	0.06	0.08
	1	0.09	0.12
	1000	0.08	0.15

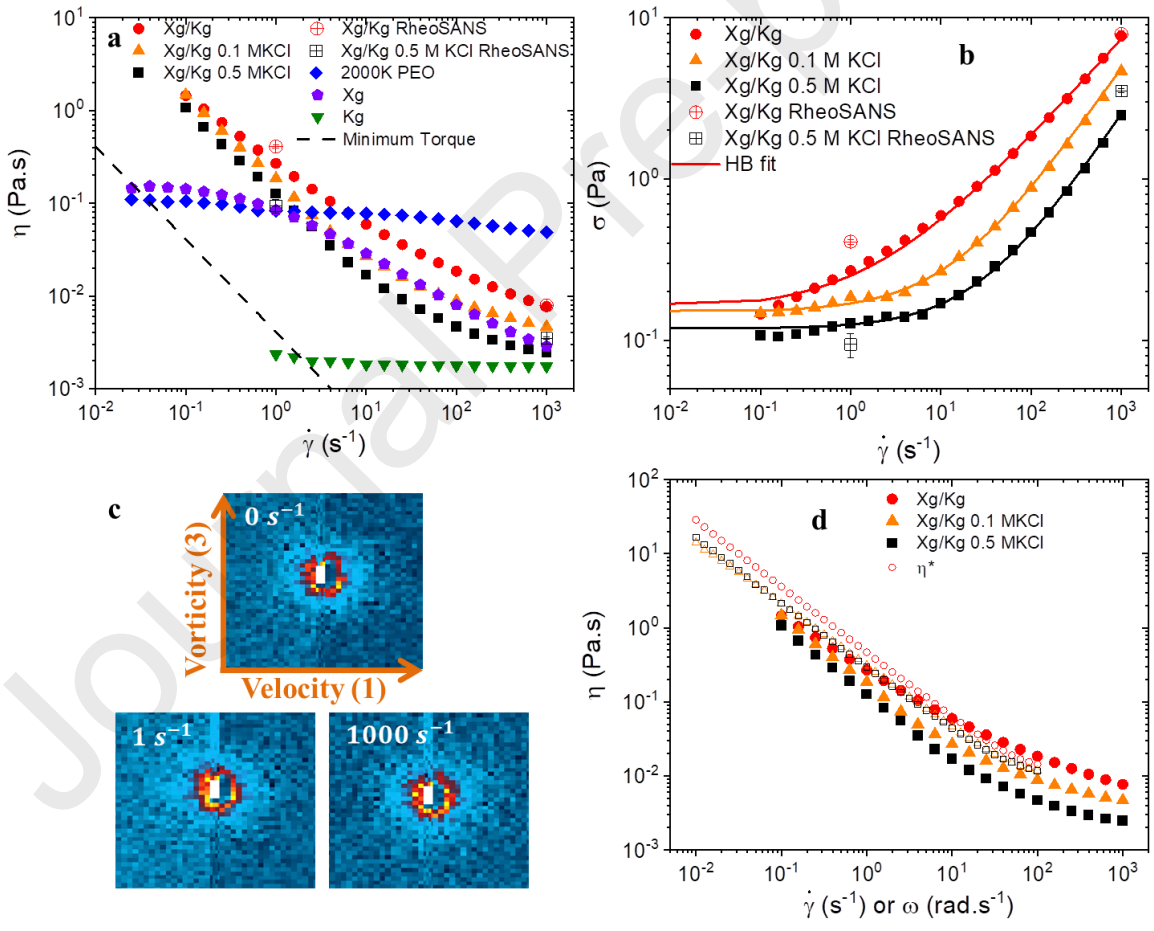

Figure 6 (a) Shear viscosity of Xg, Kg, Xg/Kg, and PEO solutions and the lower measurement limit defined by the minimum torque (dashed line). (b) Shear stress for Xg/Kg solutions with varying added electrolyte compared with corresponding Herschel-Bulkley model fitting. The hollow cross symbols are the time-averaged shear viscosity and stress obtained from rheoSANS measurements. (c)

2D patterns of neutron scattering of Xg/Kg without added KCl at rest and under shear rates of 1 and 1000 1/s. (d) The Cox-Merz rule with steady shear viscosity and complex viscosity.

3.4 Apparent Steady and Transient Extensional Rheology

Aqueous solutions of Xg/Kg both in the presence or absence of 0.1M KCl exhibit similar extensional viscosities, while Xg/Kg in the 0.5M KCl solution shows a markedly lower extensional viscosity, as presented in Figure 7a. Notably, Xg/Kg fluids have a high extensional viscosity under low rates, but show substantial extension-thinning. Similar results are reported for Xg in water and in KCl solutions [50].

The present microfluidic device has higher Hencky strain than the design (ε_H = 2) in the literature, thereby resulting in a higher shear stress component than viscoelastic component for PEO solutions. This can also be seen in the Trouton ratio as presented in Figure 7c that PEO has significant lower numbers than Xg/Kg solutions. In this regard, we plotted the literature data obtained from Ober et al. and Keshavarz et al. for 1000K, 2000K, and 4000K Mw PEO solutions also at semi-dilute concentrations, which show significant extensional-thickening as shown in Figure 7b [16, 23]. An estimate of the terminal high extension rate viscosity can be made from theory. To better understand the difference between these solutions, the finite chain extensibility (L_E) and the terminal extensional viscosity (η_E^∞) of PEO and Xg/Kg are compared in Table 7. The terminal extensional viscosity in

ultradilute solutions can be calculated using the FENE-P (finitely extensible nonlinear elastic) model for which,

$$\eta_E^{\infty} \sim 3\eta_s + 2\eta_p L_E^2 \,. \qquad (2)$$

Here, the solvent viscosity (η_s) is usually much smaller than the polymer contribution ($\eta_p L_E^2$) and η_p is the polymer contribution to the shear viscosity. Due to the higher molecular extensibility of PEO as compared to Xg/Kg solutions, the terminal extensional viscosity for these solutions are expected to be much higher.

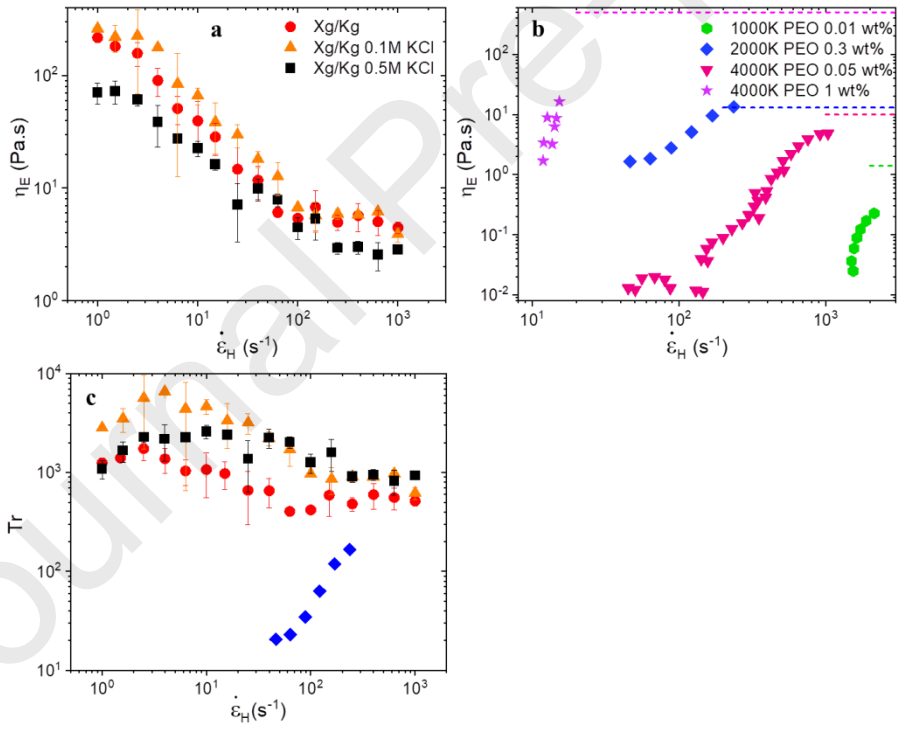

Figure 7 (a) Time-averaged extensional viscosity of Xg/Kg solutions measured using the microfluidic hyperbolic flow device as a function of Hencky extension rate. (b) Literature data of the extensional viscosity of PEO solutions. (c) Trouton ratio of Xg/Kg solutions and 2000K PEO with measured shear viscosity. Extensional data of 0.01 wt% 1000K, and 0.05 wt% and 1 wt% 4000K PEO are from Keshavarz et al. and 0.3 wt% 2000K is from Ober et al. and plotted for reference [16, 23]. The dash

line is the limiting behavior of the extensional viscosity which is the terminal extensional viscosity as listed in Table 7.

The Trouton ratio is also calculated based on the definition $Tr(\dot{\varepsilon}_H) = \eta_E^+(\dot{\varepsilon}_H)/\eta_S(\dot{\gamma})$ and $\dot{\gamma} = 2\dot{\varepsilon}_H$ for planar flow and plotted in Figure 7c [51]. An enhanced Trouton ratio, far in excess of Newtonian Trouton limit of 3, is found. This enhanced Trouton ratio is consistent with the experimental results in the literature using hydrophobic celluloses, which also form a physical network in aqueous solutions [51]. With the addition of ions, the increased finite chain extensibility can be the reason for a higher Trouton ratio at moderate extension rates, which is followed by significant extension-thinning due to the breakdown of the structure for both Xg/Kg in 0.1 M and 0.5 M KCl solutions at higher extension rates.

Table 7 Terminal extensional viscosity and extensibility of PEO and Xg/Kg

Chemical		c (wt%)	c/c^*	Finite extensibility L_E [(a)]	Terminal extensional viscosity η_E^∞ (Pa.s)[(b)]
PEO	1000K	0.01	0.07	62[(c)]	1.4 [16]
		0.17	1.26		16 [14]
		0.3	2.23		19 [14]
		0.5	3.71		36 [14]
		0.75	5.57		42 [14]
	2000K	0.3	3.5	88	13
		0.6	6.99		94 [14]
		0.75	8.74		160 [14]
		1	11.65		225 [14]
	4000K	0.05	0.91	124	10 [16]
		1	18.29		500 [16]
Xg/Kg	0M KCl	0.05	-	2.2 – 13.7	4.5
	0.1M KCl	0.05	-	3.7 – 13.7	3.9
	0.5M KCl	0.05	-	3.4 – 13.7	2.8

[(a)] Calculated using $L_E = L_c/\langle R^2\rangle_0^{0.5}$ as depicted in Table 2.
[(b)]Terminal extensional viscosity of Xg/Kg is taken at 1000 s^{-1} and the end point for 2000k PEO.
[(c)]The number is comparable to the literature value [14].

Journal Pre-proofs

While the microfluidic measurements of extensional flow are steady state in an Eulerian sense, the material element flowing through the hyperbolic contraction undergoes a transient elongation, but the device only measures the overall material behavior during this transient process. A look at the material transient behavior under uniaxial extension can be achieved using a VADER-1000. Measurements were performed for the Xg/Kg at Hencky extensional strain rates of 0.05, 0.5, and 1 s^{-1}. Here, the data of Xg/Kg solutions at 0.05 and 1 s^{-1} are plotted in Figure 8 along with the literature PEO data from Dinic and Sharma [14]. The extensional stress increases with an increased Hencky strain, i.e. extensional strain hardening behavior. In Figure 8, the y-axis shows two representations for the extensional stress due to the fact that VADER can measure the stress of Xg/Kg solutions directly while the PEO data were acquired from fitting the reduction curve of the diameter of the liquid filament. Generally, all three gum solutions show similar levels of strain hardening for the extensional rates probed. Note the highest Hencky strain rate achieved in this transient measurement is comparable to the lowest Hencky strain rate achieved in the microfluidic device. The extensional stress growth coefficients ($\overline{\eta_E^+}$) calculated from these measurements are observed to increase with an increasing Hencky strain for each solution and at each Hencky strain rate, as shown in Figure S4d-f. The growth is approximately linear. The onset of a measureable extensional viscosity shifts to a higher Hencky strain with increasing KCl. Also, note that at 1 s^{-1} the transient extensional viscosity at maximum Hencky strain is ~200 Pa-s, albeit the measurements are noisy, but these values are

comparable to the values obtained for the extensional viscosity from the microfluidic channel (Figure 7a) for these solutions.

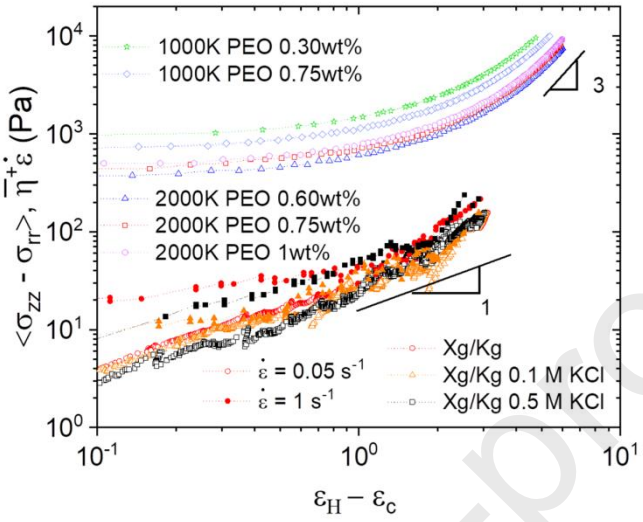

Figure 8 Transient extensional stress of Xg/Kg and PEO solutions. Measured stress-strain curves for Xg/Kg, Xg/Kg in 0.1 M KCl, Xg/Kg in 0.5 M KCl at $\dot{\varepsilon}_H = 0.05$ (open symbols) and 1 s^{-1} (solid symbols), and literature data for 1000K (0.30 and 0.75 wt%) and 2000K PEO (0.60, 0.75, and 1 wt%) are presented. Data of PEO solutions are from Dinic and Sharma [14]. Lines with scaling relationships are shown to illustrate trends in the data.

Importantly, while these gum solutions are extensional strain hardening (Figure 8), they are extensional shear rate thinning (Figure 7a). This is in contrast with the highly flexible, semi-dilute PEO solutions, which show similar extensional strain hardening (Figure 8), but rather significant extensional strain rate hardening as well (Figure 7b). It is postulated that this difference in behavior for the gum solutions is due to shear-disruption of the network structure responsible for the yield-like behavior in the viscosity, such that higher extension rates probe less-structured material. As indicated from the strong shear-thinning feature and rheoSANS data (Figure 5), the longer lengthscale microstructure of Xg/Kg tends to dissociate significantly under shear deformation without a strong

orientation, leading to a loss of network structure and shear thinning. In addition, even in the presence of significant amounts of added electrolyte, which decreases the persistence length of Xg, the solutions continue to show extensional rate thinning. Added electrolyte reduces the interaction between Xg and Kg, thereby creating a more loosely connected structure. On the other hand, flexible PEOs with significant molecular extensibility contain no physical attractions or significant cross-linked structure, but show significant strain and strain rate hardening in extensional measurements.

The yield stress of Xg/Kg solutions decreases with a broader distribution of the mesh size with increasing salt concentrations. This structure-property relationship has also been reported for carbon black systems by Hipp et al. that a loosely connected suspension has lower yield stress than a strongly connected network [48]. This reduction enables destabilization of the suspension in the Xg/Kg solutions. It is especially important in the fluid transferring process that structure breakup disables the suspension stability.

4. Conclusions

Previous studies have shown the significance of biocompatible, particle-loaded sprayable gel on the postsurgical cancer treatment and other drug delivery applications [6-8]. However, the gel was oftentimes formed after sprayed and lacks the fundamental design principles in engineering a solution that behaves like a solid below the yield stress and sprayable like water. Moreover, the sprayability of polymer suspensions has been addressed in the literature [13, 16, 51], but the fundamental understanding of the concept of spraying a yield-stress fluid with stiff and biocompatible cross-linked

Journal Pre-proofs

polymers is very limited. Here, the rheological properties of a structured polysaccharide solution with only 0.05 wt% of structuring reactants are compared to a known, flexible polymer fluid (PEO) under shear and extensional flows. The results elucidated and highlighted the importance of the tunable structural associations and molecular extensibility. Xg/Kg solutions present a yield stress and both shear- and extension-thinning, while PEO shows similar shear viscosity, but extension-thickening. The significant difference in extensional behavior is due to remarkable distinctions in molecular elasticity and the structuration in Xg/Kg solutions that is rate sensitive in both shear and extensional flows. Also, to design the desired suspension-stabilizing capability, the yield stress is required to be tunable and the polyaionic xanthan can meet this requirement. Further, adding electrolyte is shown to regulate the strength of molecular association so as to tune rheological properties. The hypothesis for the mechanism of achieving a sprayable, yield-stress fluid being due to longer-lengthscale structural breakup and low molecular extensibility is also validated by direct rheoSANS measurements of the microstructure. This understanding of the rheological properties in terms of structural and molecular information enables more effective formulation over a wider range of applications.

5. Acknowledgments

We acknowledge the financial support provided by the Procter & Gamble Company. We also thank Zachary R. Hinton and Professor Nicolas J. Alvarez for their laboratory and technical support for the transient extensional rheology, and Bob Reeder (Procter & Gamble Company) for providing the cryo-SEM images.

Journal Pre-proofs

This manuscript was prepared under cooperative agreement #370NANB17H302 and #70NANB15H260 from NIST, U.S. Department of Commerce. We acknowledge the support of the National Institute of Standards and Technology, U.S. Department of Commerce, in providing the neutron research facilities used in this work. This work utilized facilities supported in part by the National Science Foundation under Agreement No. DMR-0944772. The statements, findings, conclusions and recommendations are those of the authors and do not necessarily reflect the view of NIST or the U.S. Department of Commerce.

6. References

1. Lynch, M.L., Colina, C. J., Horenziak, S. A., Illie, B. P., Gizaw, Y., and Sun, Y., *Phase-Stable, Sprayable Freshening Compositions Comprising Suspended Particles.* December 2018(Patent US10143764B2, December 4, 2018.).

2. Bonn, D., et al., *Yield stress materials in soft condensed matter.* Reviews of Modern Physics, 2017. **89**(3).

3. Barnes, H.A., *The yield stress—a review or 'παντα ρει'—everything flows?* 1999. **81**(1-2): p. 133-178.

4. Yan, C., et al., *Injectable solid hydrogel: mechanism of shear-thinning and immediate recovery of injectable β-hairpin peptide hydrogels.* Soft Matter, 2010. **6**(20): p. 5143.

5. Annabi, N., et al., *Engineering a sprayable and elastic hydrogel adhesive with antimicrobial properties for wound healing.* Biomaterials, 2017. **139**: p. 229-243.

Journal Pre-proofs

6. Chen, Q., et al., *In situ sprayed bioresponsive immunotherapeutic gel for post-surgical cancer treatment.* Nature Nanotechnology, 2019. **14**(1): p. 89-97.

7. Mahdi, M.H., B.R. Conway, and A.M. Smith, *Development of mucoadhesive sprayable gellan gum fluid gels.* 2015. **488**(1-2): p. 12-19.

8. Shao, J., et al., *Black-Phosphorus-Incorporated Hydrogel as a Sprayable and Biodegradable Photothermal Platform for Postsurgical Treatment of Cancer.* Advanced Science, 2018. **5**(5): p. 1700848.

9. Arif Z.Nelson, K.S.S., Brittany M. Rauzan, Ralph G. Nuzzo, Jan Vermant, Randy H.Ewoldt, *Designing and transforming yield-stress fluids.* Current Opinion in Solid State and Materials Science, 2019. **23**(5).

10. Moller, P., et al., *An attempt to categorize yield stress fluid behaviour.* Philosophical Transactions of the Royal Society A: Mathematical, Physical and Engineering Sciences, 2009. **367**(1909): p. 5139-5155.

11. Ovarlez, G., et al., *Shear-induced sedimentation in yield stress fluids.* 2012. **177-178**: p. 19-28.

12. Baek, G., et al., *Atomization characteristics of impinging jets of gel material containing nanoparticles.* 2011. **166**(21-22): p. 1272-1285.

Journal Pre-proofs

13. Keshavarz, B., et al., *Studying the effects of elongational properties on atomization of weakly viscoelastic solutions using Rayleigh Ohnesorge Jetting Extensional Rheometry (ROJER).* 2015. **222**: p. 171-189.

14. Dinic, J. and V. Sharma, *Macromolecular relaxation, strain, and extensibility determine elastocapillary thinning and extensional viscosity of polymer solutions.* Proceedings of the National Academy of Sciences, 2019. **116**(18): p. 8766-8774.

15. Smith, D.E., *Response of Flexible Polymers to a Sudden Elongational Flow.* Science, 1998. **281**(5381): p. 1335-1340.

16. Keshavarz, B. and G.H. McKinley, *Micro-scale extensional rheometry using hyperbolic converging/diverging channels and jet breakup.* 2016. **10**(4): p. 043502.

17. Colby, R.H., *Structure and linear viscoelasticity of flexible polymer solutions: comparison of polyelectrolyte and neutral polymer solutions.* Rheologica Acta, 2010. **49**(5): p. 425-442.

18. Tirtaatmadja, V., G.H. McKinley, and J.J. Cooper-White, *Drop formation and breakup of low viscosity elastic fluids: Effects of molecular weight and concentration.* 2006. **18**(4): p. 043101.

19. Georgelos, P.N. and J.M. Torkelson, *The role of solution structure in apparent thickening behavior of dilute peo/water systems.* 1988. **27**(2): p. 191-204.

20. Perazzo, A., et al., *Flow-induced gelation of microfiber suspensions.* Proceedings of the National Academy of Sciences, 2017. **114**(41): p. E8557-E8564.

Journal Pre-proofs

21. Spagnolie, S.E., *Complex Fluids in Biological Systems: Experiment, Theory, and Computation*. 2015: Springer New York.

22. Squires, T.M. and S.R. Quake, *Microfluidics: Fluid physics at the nanoliter scale.* Reviews of Modern Physics, 2005. **77**(3): p. 977-1026.

23. Ober, T.J., et al., *Microfluidic extensional rheometry using a hyperbolic contraction geometry.* Rheologica Acta, 2013. **52**(6): p. 529-546.

24. Haward, S.J., et al., *Optimized Cross-Slot Flow Geometry for Microfluidic Extensional Rheometry.* 2012. **109**(12).

25. Kim, M.M., et al., *The improved resistance of PDMS to pressure-induced deformation and chemical solvent swelling for microfluidic devices.* Microelectronic Engineering, 2014. **124**: p. 66-75.

26. Stokes, J.R., et al., *Lubrication, Adsorption, and Rheology of Aqueous Polysaccharide Solutions.* Langmuir, 2011. **27**(7): p. 3474-3484.

27. Lee, S., et al., *Influence of Molecular Architecture on the Adsorption of Poly(ethylene oxide)−Poly(propylene oxide)−Poly(ethylene oxide) on PDMS Surfaces and Implications for Aqueous Lubrication.* Macromolecules, 2004. **37**(22): p. 8349-8356.

28. Thielicke, W. and E.J. Stamhuis, *PIVlab – Towards User-friendly, Affordable and Accurate Digital Particle Image Velocimetry in MATLAB.* Journal of Open Research Software, 2014. **2**.

29. Ayachit, U., *The ParaView Guide: A Parallel Visualization Application* 2015: Kitware, Inc.

Journal Pre-proofs

30. Bustamante, C., et al., *Entropic elasticity of lambda-phage DNA.* Science, 1994. **265**(5178): p. 1599-1600.

31. Marko, J.F. and E.D. Siggia, *Stretching DNA.* Macromolecules, 1995. **28**(26): p. 8759-8770.

32. Larson, R.G., *The rheology of dilute solutions of flexible polymers: Progress and problems.* 2005. **49**(1): p. 1.

33. Lee, H., et al., *Molecular Dynamics Studies of Polyethylene Oxide and Polyethylene Glycol: Hydrodynamic Radius and Shape Anisotropy.* Biophysical Journal, 2008. **95**(4): p. 1590-1599.

34. Kök, M.S., et al., *A novel global hydrodynamic analysis of the molecular flexibility of the dietary fibre polysaccharide konjac glucomannan.* 2009. **23**(7): p. 1910-1917.

35. Camesano, T.A. and K.J. Wilkinson, *Single Molecule Study of Xanthan Conformation Using Atomic Force Microscopy.* Biomacromolecules, 2001. **2**(4): p. 1184-1191.

36. Donets, S. and J.-U. Sommer, *Molecular Dynamics Simulations of Strain-Induced Phase Transition of Poly(ethylene oxide) in Water.* The Journal of Physical Chemistry B, 2018. **122**(1): p. 392-397.

37. Norton, I.T., et al., *Mechanism and dynamics of conformational ordering in xanthan polysaccharide.* Journal of Molecular Biology, 1984. **175**(3): p. 371-394.

38. Israelachvili, J.N., *Intermolecular and surface forces*. 2015: Academic press.

Journal Pre-proofs

39. Fitzpatrick, P., et al., *Control of the properties of xanthan/glucomannan mixed gels by varying xanthan fine structure.* Carbohydrate Polymers, 2013. **92**(2): p. 1018-1025.

40. Morris, E.R., *Ordered conformation of xanthan in solutions and "weak gels": Single helix, double helix – or both?* Food Hydrocolloids, 2019. **86**: p. 18-25.

41. Annable, P., P.A. Williams, and K. Nishinari, *Interaction in Xanthan-Glucomannan Mixtures and the Influence of Electrolyte.* Macromolecules, 1994. **27**(15): p. 4204-4211.

42. Song, K.-W., Y.-S. Kim, and G.-S. Chang, *Rheology of concentrated xanthan gum solutions: Steady shear flow behavior.* Fibers and Polymers, 2006. **7**(2): p. 129-138.

43. Abbaszadeh, A., et al., *New Insights into Xanthan Synergistic Interactions with Konjac glucomannan: A Novel Interaction Mechanism proposal.* 2016.

44. Erk, K.A., et al., *Extreme Strain Localization and Sliding Friction in Physically Associating Polymer Gels.* Langmuir, 2012. **28**(9): p. 4472-4478.

45. Gennes, P.-G.d., *Scaling concepts in polymer physics*. 1979, Ithaca, N.Y.: Cornell University Press.

46. Pochan, D.J., et al., *SANS and Cryo-TEM Study of Self-Assembled Diblock Copolypeptide Hydrogels with Rich Nano- through Microscale Morphology.* Macromolecules, 2002. **35**(14): p. 5358-5360.

47. Rosenblatt, J., B. Devereux, and D.G. Wallace, *Injectable collagen as a pH-sensitive hydrogel.* 1994. **15**(12): p. 985-995.

Journal Pre-proofs

48. Hipp, J.B., J.J. Richards, and N.J. Wagner, *Structure-property relationships of sheared carbon black suspensions determined by simultaneous rheological and neutron scattering measurements.* Journal of Rheology, 2019. **63**(3): p. 423-436.

49. Smith, D.E., *Single-Polymer Dynamics in Steady Shear Flow.* Science, 1999. **283**(5408): p. 1724-1727.

50. Martín-Alfonso, J.E., et al., *Relation between concentration and shear-extensional rheology properties of xanthan and guar gum solutions.* Carbohydrate Polymers, 2018. **181**: p. 63-70.

51. Sharma, V., et al., *The rheology of aqueous solutions of ethyl hydroxy-ethyl cellulose (EHEC) and its hydrophobically modified analogue (hmEHEC): extensional flow response in capillary break-up, jetting (ROJER) and in a cross-slot extensional rheometer.* 2015. **11**(16): p. 3251-3270.

Journal Pre-proofs

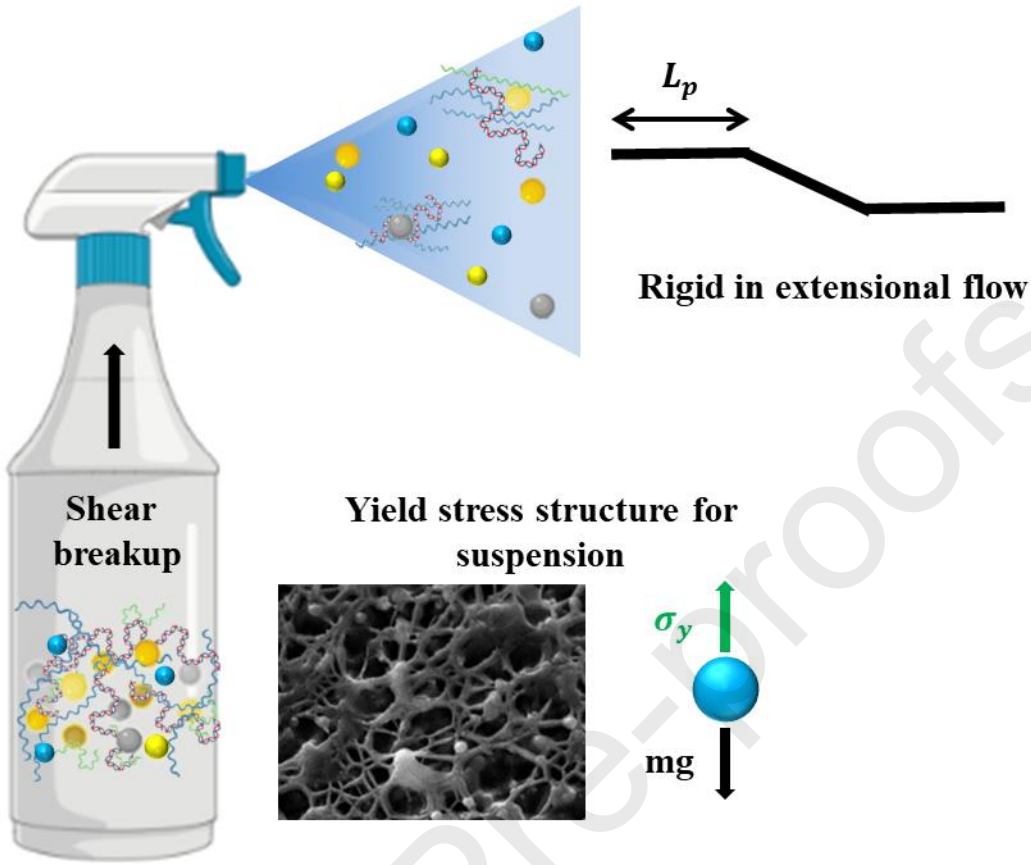

Molecular engineering of thixotropic, sprayable fluids with yield stress using associating polysaccharides

Yu-Jiun Lin[1], Jeffrey Horner[1], Brandon Illie[2], Matthew L. Lynch[2], Eric M. Furst[1], and Norman J. Wagner[1]

Yu-Jiun Lin: Conceptulization, Methodology, Investigation, Formal Analysis, Writing – Original Draft, Writing Review and Editing.
Jeffrey Horner: Formal Analysis.
Brandon Illie: Investigation, Resources.
Matthew Lynch: Conceptulization, Investigation, Resources, Writing – Original Draft, Writing Review and Editing, Supervision, Project Administration, Funding Acquisition.
Eric M. Furst: Supervision, Project Administration, Writing – Review and Editing.
Norman Wagner: Supervision, Project Administration, Writing – Review and Editing.

Journal Pre-proofs